Open access • Journal Article • DOI:10.1007/S12633-021-01420-W

Design and Investigation of F-Shaped Tunnel FET With Enhanced Analog/RF Parameters — Source link

Prabhat Singh, Dharmendra Singh Yadav

Institutions: National Institute of Technology, Hamirpur

Published on: 29 Sep 2021 - Silicon (Springer Netherlands)

Topics: AND gate, Threshold voltage, Capacitance, Voltage and Parasitic capacitance

Related papers:

- Drive current enhancement in TFET by dual source region
- Performance Analysis of Vertically Stacked Nanosheet Tunnel Field Effect Transistor with Ideal Subthreshold Swing
- A novel vertical tunneling based Ge-source TFET with enhanced DC and RF characteristics for prospect low power applications
- A Novel Extended Source TFET with δp+- SiGe Layer
- Extended-Source Double-Gate Tunnel FET With Improved DC and Analog/RF Performance

Share this paper:

View more about this paper here: https://typeset.io/papers/design-and-investigation-of-f-shaped-tunnel-fet-with-2bv5l66txb

Design and investigation of F-shaped Tunnel FET with enhanced Analog/RF parameters

Prabhat Singh, Dharmendra Singh Yadav

***Abstract*—In this manuscript, a novel physically doped single gate F-shaped tunnel FET is simulated and optimized. The designed configuration is well optimized and analyzed for different source thickness, source length, drain length with different lateral tunneling lengths between the source edge and gate dielectric. Also, we optimized some stand-points like threshold voltage, I_{ON} to I_{OFF} current ratio, ambipolar conduction range, sub-threshold swing and various capacitance to rectify the analog/RF performance of single gate F-shaped TFET. Regarding this, we concurrently optimize the lateral tunneling length between source and gate with optimization of source thickness. The variation in lateral tunneling length, the potential and strength of electric field at fixed V_{gs} voltage is varied which leads to effective change in the ON-current, average sub-threshold swing, and turn ON-voltage. Another side, as well as the source thickness vary, the electric field variation takes place near the edge of source, which leads to variation in the ON-current and ON-voltage. The performance parameters of single gate F-TFET is compared with single gate L-TFET, which is the incentive of this submitted work. The optimized single gate F-TFET have 0.30 V turn ON-voltage with 7.4 mV/decade average sub-threshold swing and high I_{on}/I_{off} ratio approx 10^{13}. Besides, a significant reduction in parasitic capacitance is beneficial to enhanced RF performance with better controllability on channel.**

***Index Terms*—Ambipolar conduction, Sub-threshold conduction, Band-to-Band-Tunneling, F-shaped channel, L-shaped channel.**

I. INTRODUCTION

TO get the better of MOSFET, Tunnel FET (TFET) has been brought in as an auspicious candidate for a low power application because its sub-threshold swing (SS) can be scaled down than 60 mV/dec [1], [2]. At the initial, the Si-based single gate Tunnel FET experience very low I_{ON} with high ambipolar conduction because of approximately same band-to-band (B2B) tunneling on both drain/channel and source/channel interface [3]. Furthermore, Dual-Gate TFET (DG-TFET) was introduced for better channel controllability to improve the I_{ON} current but again the ambipolar conduction is a major issue [4]. Likewise, various type of techniques and strategies have been proposed to overcome the ambipolar behavior of Tunnel FET device [5]–[7]. Furthermore, there is some limited research article that has improved I_{ON} and suppressed ambipolar conduction with reduced average sub-threshold swing (SS_{avg}) by increasing BTBT region [8], [9]. Some of them, various structure/shape of TFET has been proposed to achieve the improved result in comparison to the previous one [10]–[12]. As well as the new structure came into existence, some parameter optimization also came into the picture like Threshold voltage (V_T), gate-to-drain capacitance (C_{gd}), gate-to-source capacitance (C_{gs}), cut-off frequency (f_t), Gain Bandwidth product (GBP), transit time etc.

For the low power application, we need low V_{ON}, which is defined as minimum gate-to-source voltage (V_{gs}) at which a transition path has been created between the source and drain region [13]. A novel device structure for low power application named as single gate F-shaped TFET (SG-F-TFET) has been proposed and optimize which consists highly doped source enclosed by a lightly doped silicon region. With the help of the electric field crowding effect, the SG-F-TFET is supposed to minimize V_{ON} as the source thickness is decreased [14], [15]. 2D TCAD tool is used to simulate and analyses the analog/RF properties of the SG-F-TFET.

II. SCHEMATIC AND SPECIFICATIONS OF DESIGNED DEVICE

The 2D schematics of DG-TFET, Hetero Material DG-TFET (HMDG-TFET), Single Gate L-shaped TFET (SG-L-TFET), and Single Gate F-shaped TFET (SG-F-TFET) are set out in Fig. 1a-1d respectively. TableI lists the basic device dimension parameters used for carrying out TCAD simulations. The simulated structures uses physical doping techniques to introduce the dopants in the device. In Fig.1a, a low-k gate oxide (SiO_2) based homo double gate TFET structure is shown which consist Si/Si/Si semiconductor material for source, channel, and drain respectively with L_S = 55 nm, L_C = 50 nm, L_D = 55 nm and t_{OX} = 1 nm. Further, in Fig.1b, a schematic of high-k gate oxide based hetero double gate TFET shown which consist Si/GaAs/GaAs semiconductor material for source/channel/drain region respectively. The higher bandgap material (GaAs) is used in channel and drain region to eradicate, the ambipolar conduction. For further analysis, SG-L-TFET is simulated with source thickness 35 nm and drain thickness is set to 6 nm with oxide thickness 1 nm, considering these the ambipolar conduction is suppressed but the turn ON-voltage is quite high (Fig.1c). So, a new device structure, SG-F-TFET is proposed to decimate the limitation of all previous simulated devices.

A physical doping-based SG-F-TFET is simulated and analyzed for the various device and analog parameters. This simulated structure called ”F-shaped” because its channel resembles the finger like source and its 2-D cross sectional view shown in Fig.1d. Different colors are shown in Fig.1d define

Prabhat Singh, Electronics and Communication Engineering Department, NIT Hamirpur, Himanchal Pradesh, 177005 India, e-mail: prabhat@nith.ac.in

Dharmendra Singh Yadav,Electronics and Communication Engineering Department, NIT Hamirpur, Himanchal Pradesh, 177005 India, e-mail: dsyadav@nith.ac.in

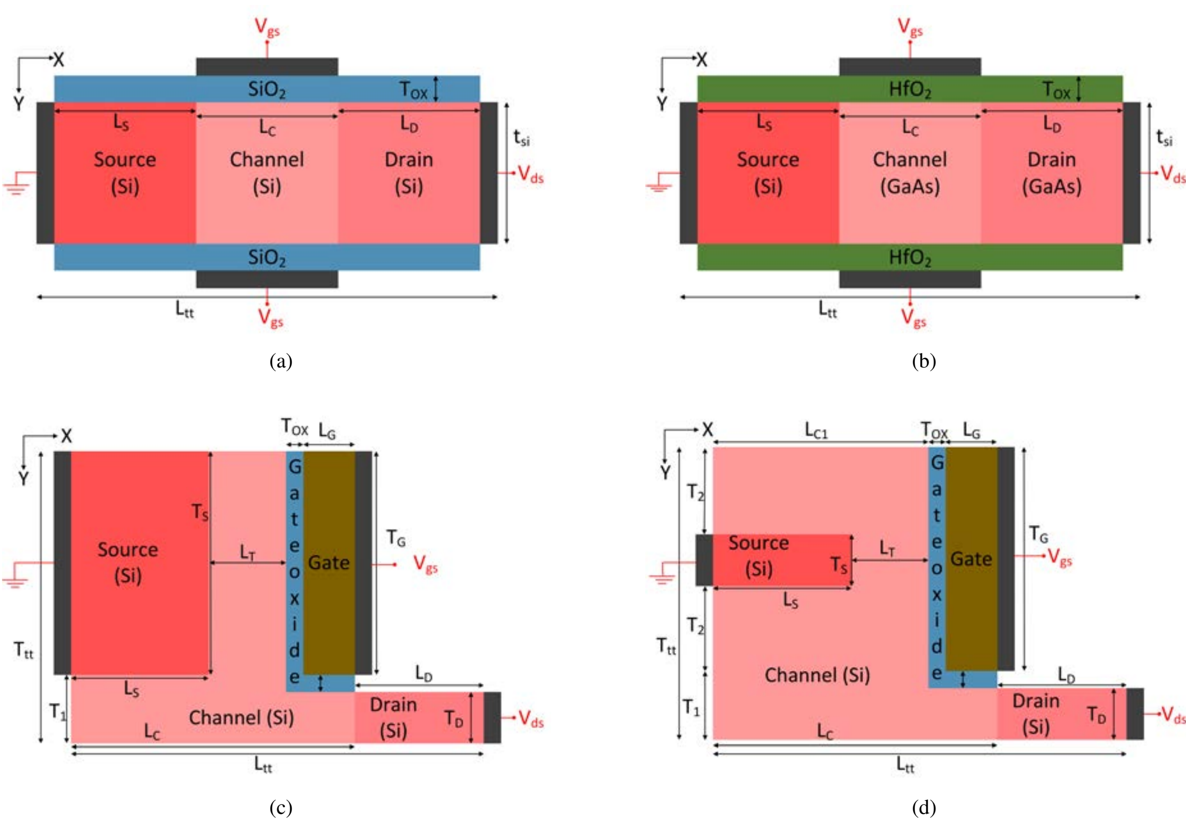

Fig. 1. The general 2D graphic of (a) DG-TFET (b) Hetero material DG-TFET (HMDG-TFET) (c) Single-gate L-shaped TFET (SG-L-TFET) and (d) Single-gate F-shaped TFET (SG-F-TFET) with T_{OX} = 1 nm

TABLE I
DESCRIPTION OF THE BASIC DESIGN VARIABLES WHICH ARE USED FOR THE TCAD SIMULATION

Parameters	Abbreviations	DG-TFET	HMDG-TFET	SG-L-TFET	SG-F-TFET
Gate oxide thickness	T_{OX}	1 nm	1 nm	1 nm	1 nm
Gate oxide material (k-value)	–	SiO_2 (k=3.9)	HfO_2 (k=22)	SiO_2 (k=3.9)	SiO_2 (k=3.9)
Total device length	L_{tt}	160 nm	160 nm	160 nm	160 nm
Thickness above and below source	T_2	–	–	–	Variable (12.5 nm)
Channel thickness at bottom of device	$T_1 = T_D + T_{OX}$	–	–	7 nm	7 nm
Total device thickness	T_{tt}	12 nm	12 nm	42 nm	42 nm
Lateral tunneling length	L_T	–	–	4 nm	Variable (4 nm)
Source thickness	T_S	10 nm	10 nm	35 nm	Variable (10 nm)
Source length	L_S	55 nm	55 nm	67 nm	Variable (67 nm)
Gate length	L_G	50 nm	50 nm	20 nm	20 nm
Gate thickness	$T_G = 2T_2 + T_S$	–	—	35 nm	35 nm
Channel thickness	$2T_2 + T_1 + T_S$	10 nm	10 nm	42 nm	42nm
Channel length (upper)	L_{C1}	50 nm	50 nm	71 nm	71 nm
Channel length (bottom)	L_C	50 nm	50 nm	92 nm	92 nm
Drain length	L_D	55 nm	55 nm	68 nm	68 nm
Drain thickness	T_D	10 nm	10 nm	6 nm	6 nm
Gate work-function	WF_G	4.5 eV	4.5 eV	4.5 eV	4.5 eV
N-type drain doping concentration	N_D	$10^{18}\ cm^{-3}$	$10^{18}\ cm^{-3}$	$10^{18}\ cm^{-3}$	$10^{18}\ cm^{-3}$
P-type channel doping concentration	N_C	$10^{15}\ cm^{-3}$	$10^{15}\ cm^{-3}$	$10^{15}\ cm^{-3}$	$10^{15}\ cm^{-3}$
P-type source doping concentration	N_S	$10^{20}\ cm^{-3}$	$10^{20}\ cm^{-3}$	$10^{20}\ cm^{-3}$	$10^{20}\ cm^{-3}$

gate oxide, drain, source,channel regions, and electrodes. SG-F-TFET resembles an ultra-thin highly doped source that is enclosed by lightly doped silicon regions. For analysis and simulations, the doping levels were 1x$10^{20} cm^{-3}$, 1x$10^{18} cm^{-3}$ and 1x$10^{15} cm^{-3}$ for the source, drain, and channel regions respectively with 4.5 eV gate work function (WF_G).

The simulation of designed devices is carried out on 2D device simulator TCAD tool [16]. To appropriate internal operation of devices, nonlocal band to band (B2B) tunneling model is used to incorporate the quantum tunneling phenomena at SCIn (source/channel interface) and DCIn (channel/drain interface) by defining quantum tunneling region (qt region) for accurate tunneling process of charge carriers at both interfaces. Excluding this, FERMI and FERMI.NI models are also used

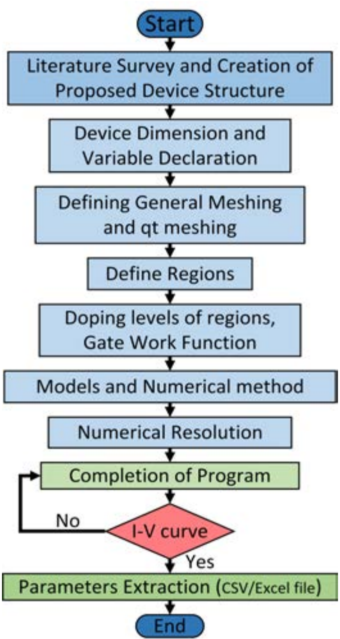

Fig. 2. Flow chart for simulation on TCAD tool

to satisfy the Fermi Dirac distribution characteristics. During the simulation, the Shockley-Read-Hall (SRH) recombination, auger, CONMOB, BGN, and FLDMOB models were implemented in addition to the trap assistant tunneling model.

III. Device analysis procedure and analog/RF parameters

A. Device analysis procedure

The vertical and lateral device dimension is chosen carefully during simulation process to compare the proposed device performance w.r.t to other simulated devices which were optimized earlier by researchers. In addition with, fine messing is defined near drain/channel and source/channel interface where B2B tunneling takes place. Mesh size near B2B tunneling interface is set to $1\times10^{-4}\mu m$ and mesh size = $5\times10^{-3}\mu m$ far of interface. The nonlocal B2B tunneling model was applied with Newton's numerical method based on iteration (up to 25 iterations) for better convergence of current [4], [17]. Excluding this, to analyze RF functioning, a small signal AC analysis was performed by setting frequency at 1 MHz. The generalized decision making flow chart for device simulation is shown in Fig.2.

B. Details of device analog/RF parameters

This sub-section is considered for a concise front matter about analog/RF performance parameters e.g. Transconductance (g_m), f_t, GBP, Transconductance Generation Factor (TGF), Transconductance Frequency Product (TFP), Transit time (τ), and parasitic capacitance (C_{gd} and C_{gs}) [18].

$$C_{gd} = \frac{\partial Q_s}{\partial V_{gd}} \tag{1}$$

$$C_{gs} = \frac{\partial Q_s}{\partial V_{gs}} \tag{2}$$

A mathematical expression of C_{gd} and C_{gs} has given in equations 1 and 2 which play a pivotal role to extract device performance and responsible for parasitic oscillation at various operating frequencies. The first order differentiation of drain current (I_{ds}) w.r.t. V_{gs} is known as g_m, convey in equation 3. The value of g_m is used to check the device speed. A higher value g_m, faster switching response of device [19].

$$g_m = \frac{\partial I_d}{\partial V_{gs}} \tag{3}$$

Another important device parameter is f_t, it is the max. frequency at which a given device works properly without any performance debasement. f_t is also interpreted as an operating frequency at which short circuit gain becomes equal to unity. To analyses, the f_t parameter of device w.r.t to parasitic capacitances, the relation between both is given in equation 4.

$$f_t = \frac{g_m}{2\pi(C_{gs}+C_{gd})} \tag{4}$$

The mathematical expression for GBP is given by equation 5. As per equation, it is directly in proportion to g_m value and inversely proportional to C_{gd} value of the device [20], [21]. A high value of GBP is required for superior high frequency performance.

$$GBP = \frac{g_m}{2\pi C_{gd}} \tag{5}$$

TGF and TFP are substantial parameters to account for device efficiency and the trade-off between power dissipation and operating bandwidth respectively. Both device parameter values should be high for low power circuit operation with high speed. The mathematical equations of TGF and TFP are given by equation.6 and 7 respectively [5], [22], [23].

$$TGF = \frac{g_m}{I_d} \tag{6}$$

$$TFP = \frac{g_m f_t}{I_d} \tag{7}$$

Another crucial operational factor for RF analysis is transit time which is defined as the time requires to charge carriers to be shifted from source to channel, given by equation 8. According to this mathematical equation, transit time is inversely proportional to f_t. If the f_t value increases the transition time decreases [24].

$$\tau = \frac{1}{2\pi f_t} \tag{8}$$

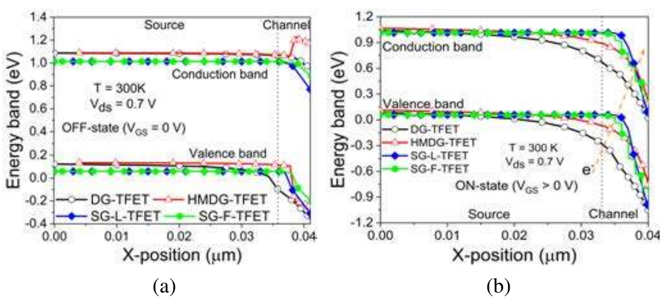

Fig. 3. Analysis of EBD (Energy band-diagrams) (a) OFF-state, V_{ds} = 0.7 V with V_{gs} = 0.0 V and (b) ON-state, V_{ds} = 0.7 V with V_{gs} = 1.5 V at SCIn for the schematic mention in Fig.1

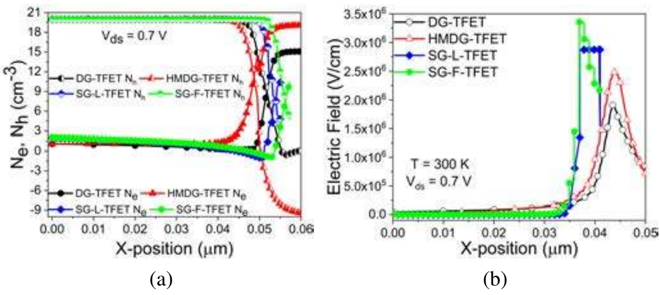

Fig. 4. Device schematic corresponds to Fig.1 (a) Comparison of charge carrier concentration and (b) Electric field at SCIn and room temperature.

IV. Simulation Results and observations

A. Performance analysis of devices

This section edifies the impact of the shape of source and channel regions on the performance of physically doped TFET. For this, the effect can be observed on alignment of energy bands and strength of electric field. At room temperature (T = 300 K), energy band alignment at source/channel interface (SCIn) is approximately close for all simulated device structures for OFF-state condition because week electric field is present without V_{gs} application (Fig. 3a). On the other hand, at T = 300 K, $V_{gs} > 0V$ is applied (ON-state condition), the source's VB (Valence band) and channel's CB (Conduction band) get aligned. From Fig. 3b, band alignment for DG-TFET and HMDG-TFET is close enough. Similarly for the SG-L-TFET and proposed device. Along with, a relative electron and hole concentration of all devices are shown in Fig.4a at same doping levels. The electric field strength at SCIn is different for all devices because of the change in shape of source and the use of hetero material (Fig.4b). The electric field strength for proposed device is significantly large compared to other simulated devices. This effect is reflected in terms of high ON-current with low V_{ON} for the SG-F-TFET, as shown in Fig.5.

B. Analog and High Frequency Performance with Parametric Variation

1) Impact of Lateral Tunneling Length (L_T): The initially designed SG-F-TFET was simulated by varied the L_T from 10 nm to 2 nm, to analyze the impact on I_{ON}/I_{OFF} ratio, ambipolar current (I_{ambi}), V_{ON} voltage and analog/RF

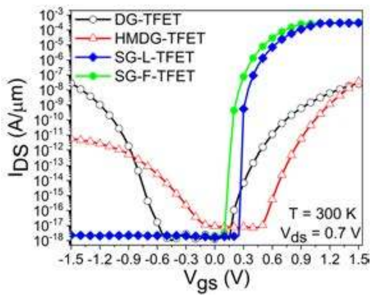

Fig. 5. Comparison of simulated SG-F-TFET transfer characteristics with DG-TFET, HMDG-TFET, and SG-L-TFET, all the devices have t_{ox} = 1 nm L_{tt} = 120 nm.

parameters. Fig. 6a shows the EBD for different L_T along the channel direction at thermal equilibrium condition. In this Fig.6a, the steepness of tunneling junction in not significantly affected by L_T variation but at other hand the electric field strength at SCIn diminished as well as L_T value is increases. Due to increment in L_T value the surface potential at fixed gate to source voltage is decrease which impact shown in term of reduced electric field (up to $2.3\times10^6\ V/cm$) (Fig. 6b). This can effect the I_{ON} range because a high electric field helps to achieve better B2B tunneling rate [25], [26]. In this concern, a comparison between $I_{ds} - V_{gs}$ characteristics for different

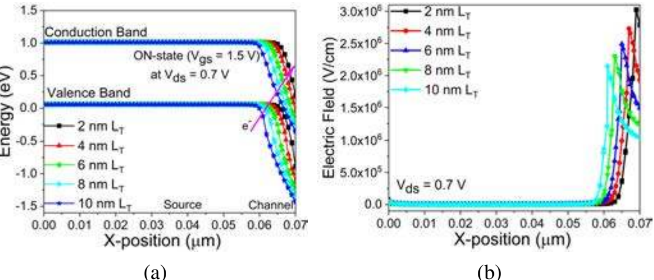

Fig. 6. Device schematic corresponds to Fig. 1d (a) Data plot of EBD of the ON-state condition, and (b) Electric field variation data plot at different tunneling length (L_T)

values of L_T is presented in Fig. 7. For significant observation related to ON-current variation, $I_{ds} - V_{gs}$ curve is plotted on linear axis (Fig.7, Y-axis, Right-hand). Along with, $I_{ds} - V_{gs}$ curve also plotted on log scale (Fig.7, Y-axis, Left-hand) for extraction of SS_{avg} and V_{ON} of proposed device.

The $I_{ds} - V_{gs}$ curve of proposed device is shifted towards the lower V_{gs} value on x-axis, which indicates that V_{ON} is reduced with miniaturization in lateral tunneling length because of potential value at fixed V_{gs} is reduced [27], [28]. Along with, the steepness of $I_{ds} - V_{gs}$ curve also improved as L_T reduces, it is imputed to the smaller tunneling width at 2 nm and 4 nm L_T. Likewise, I_{ON} increases as L_T decreases (Fig.7), because of decreased tunneling width for ON-state condition. The I_{ambi} of proposed device is not much affected by the L_T because ambipolar behavior of TFET mainly depends on the drain/channel interface (DCIn) [29] and L_T does not affect this interface in this proposed work.

The gate-gate capacitance is mainly composed of two capacitances C_{gd} and C_{gs}, shown in Fig.8 [24]. A significant

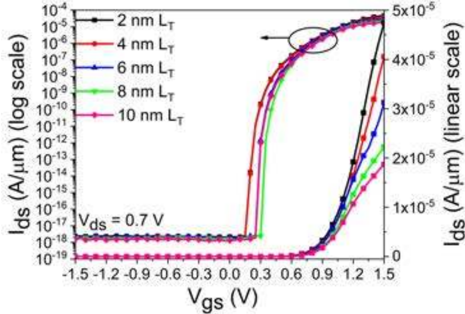

Fig. 7. Comparison of transfer characteristics of SG-F-TFET for L_T (2 nm to 10 nm) at fixed T_S = 10 nm for both log (Left y-axis) and linear scale (Right y-axis).

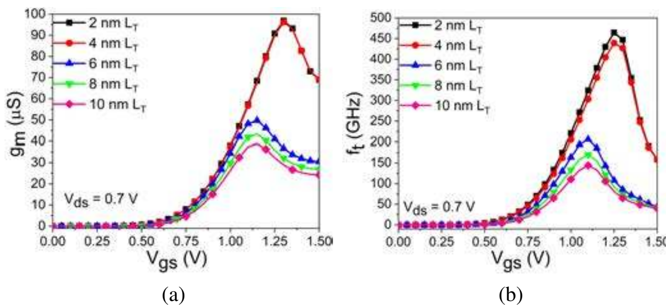

Fig. 9. Analysis of (a) g_m and (b) f_t for different L_T values

reduction in capacitances is reflected with decrease L_T because of high tunneling effect which reduces the carrier accumulation rate. The C_{gd} is a dominant capacitance due to the accumulation of the electron of channel-source and collected by the drain region [30], [31]. The finger like source helps to reduce the capacitances by reducing the accumulation of opposite type charge carrier near channel-source and channel-drain interfaces. The reduced value of C_{gd} helps to attain superior gate controllability over the channel region. The C_{gd} value of SG-F-TFET is reduced up to 0.5 fF at L_T = 2 nm and 4 nm because of reduced drain-channel interface (6 nm), as shown in Fig.8a. As shown in Fig.8b, the reduced value of L_T reflected in terms of decreased C_{gs} because of high tunneling at SCIn. In addition to C_{gd}, C_{gs} is also a parameter of interest for high-frequency introspection of device operations.

From Fig.9a, the SG-F-TFET achieves a higher transconductance (g_m) value at the higher V_{gs} for L_T = 2 nm and 4 nm due to high steepness of I_{ds}-V_{gs} curve, whereas g_m starts decreasing after achieving the peak because of less variation in I_{ds} w.r.t V_{gs} as mention in equation 3. The high frequency performance of the proposed device was analyzed by f_t and GBP [32]. The f_t can be evaluated by the ratio of g_m to C_{gg} (C_{gd}+C_{gs}) as mention in equation 4. A higher range of f_t is achieved for L_T = 2 nm and 4 nm at higher value of V_{gs} due to high g_m at higher V_{gs} and reduced total capacitance (C_{gg}) in comparison to other high values of L_T, mention in Fig. 9b. After attaining its maximum value, f_t graph starts decreasing because of the higher value of C_{gd} for $V_{gs} > 1.25\ V$ [27], [33], [34]. Along with, GBP is higher for the L_T = 2 nm and 4 nm by the effect of lower C_{gd} (Fig.8a) value as shown in Fig. 10a.

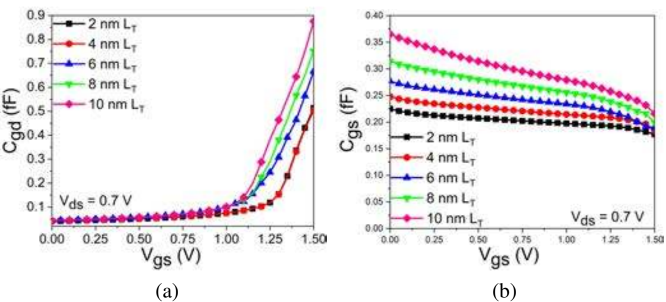

Fig. 8. Analysis of (a) C_{gd} and (b) C_{gs} for different L_T values

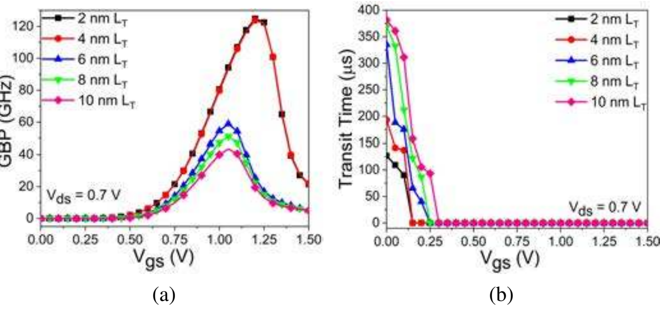

Fig. 10. Data plot of (a) GBP and (b) Transit time (τ) for different L_T values at T_S = 10 nm for proposed device.

Another remarkable RF analysis performance parameter is transit time, which is inversely proportional to f_t value. The transit time is decreased when f_t increases. For a lower value of transit time, speed of the device is improved [2]. From Fig.10b, it can be analyzed that, transit time is very less for L_T = 2 nm for lower V_{gs}. But for the higher V_{gs} value, it is similar for all L_T variations.

The TFP and TGF curve with L_T variation is shown in Fig.11. For L_T = 2 nm/4 nm we get very high TFP, which helps to enhance the device speed with low power consumption [35]. Fig.11b communicate the TGF variation for all L_T value. For 2 nm and 4 nm of L_T, TGF is maximum in sub-threshold region for $V_{gs} > 0.8\ V$. So proposed device with L_T = 2 nm or 4 nm can be used effectively for switching applications. Considering the above analysis based on L_T variation, the optimum L_T is set to either 2 nm or 4 nm, since the increase in I_{ON}, V_{ON}, SS_{avg} with improved analog/RF parameter. To select the optimum value of L_T = 2 nm or 4 nm. We have performed further analysis on the source thickness by setting L_T = 2 nm and 4 nm.

2) Impact of Source Thickness (T_S) at 2 nm L_T: In the previous section, we analyzed the effect of lateral tunneling length on SG-F-TFET. We will examine the impact of source thickness on the proposed device performance by considering two cases:

I. Source Thickness (T_S) at 2 nm L_T
II. Source Thickness (T_S) at 4 nm L_T

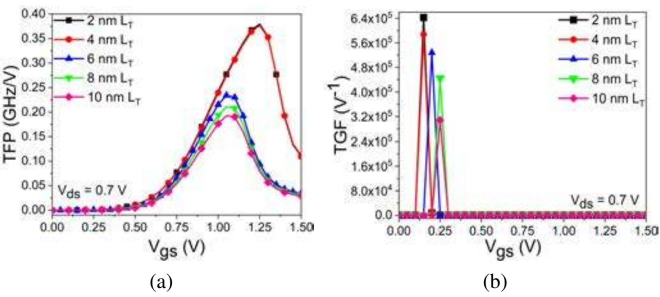

(a) (b)

Fig. 11. (a) TFP and (b) TGF data plot for different L_T values at T_S = 10 nm for proposed device.

In this section, the consequences of T_S variation on analog/RF parameters are analyzed at L_T = 2 nm. Fig.12 shows the $I_{ds} - V_{gs}$ curve depending on T_S and L_T set to 2 nm. From this graph, we can see that, as T_S is increasing, the I_{ON} is decreasing with a very small variation in I_{ambi} and V_{ON}. The I_{ON} decreases because of electric field crowding effect at the edges of the source regions decreases as well as the T_S increases i.e., the electric field at SCIn is the sum of two component, field at corner of source region (E_C) and the flat region of source (E_F). As the T_S increases, the effect of E_C field component is minimized, so a significant reduction can be seen in the I_{ds} value, as mention in Fig.12.

Fig 13 shows the capacitances for various T_S values. The C_{gd} curve is increasing from low to high V_{gs} (0 - 1.5 V). As the T_S increases, the accumulation of electron carriers is increased at SCIn which are collected by the drain region. So, the C_{gd} increases as source thickness increases, as revealing in Fig.13a. Apart from this, the same effect is reflected in the C_{gs} capacitance data plot as shown in Fig.13b.

The g_m value of a device depends on the change in I_{ds} w.r.t V_{gs}. The change in I_{ds} is higher for lower gate voltage, for the decreasing value of T_S. Hence, the improved g_m achieved at 3 nm source thickness, shown in Fig.14a. The high frequency performance is investigated by using two important parameters f_t and GBP. The higher f_t archives at 3 nm source thickness due to the high g_m at higher V_{gs} as well as the reduced value of C_{gg} (Fig.14b). The GBP is also high, when T_S is set to 3 nm by the effect of reduced C_{gd} for T_S = 3 nm, mention in Fig15a.

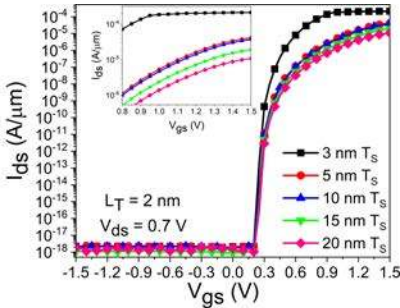

Fig. 12. Simulated SG-F-TFET transfer characteristics for different T_S values at L_T = 2 nm. Inset: a zoomed graph of $I_{ds} - V_{gs}$ curve for clear verification of impact of T_S at fixed L_T.

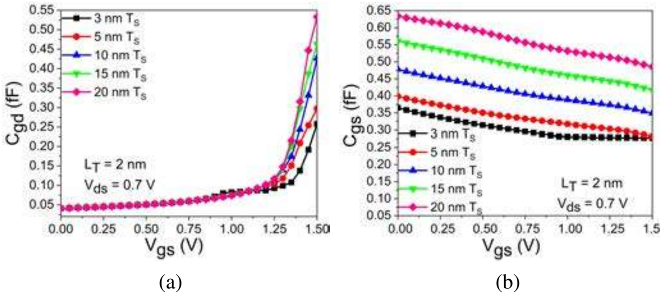

(a) (b)

Fig. 13. Analysis of (a) C_{gd} and (b) C_{gs} for T_S = 3 nm to 20 nm at L_T = 2 nm for proposed device.

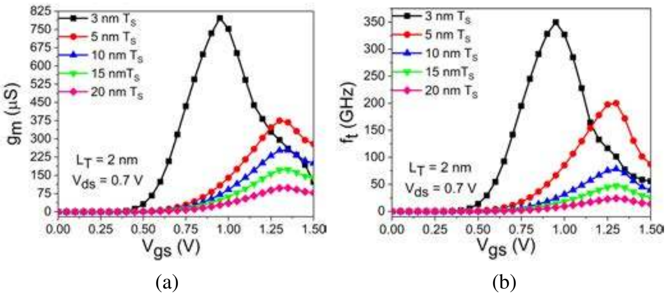

(a) (b)

Fig. 14. Analysis of (a) g_m and (b) f_t for T_S = 3 nm to 20 nm at L_T = 2 nm

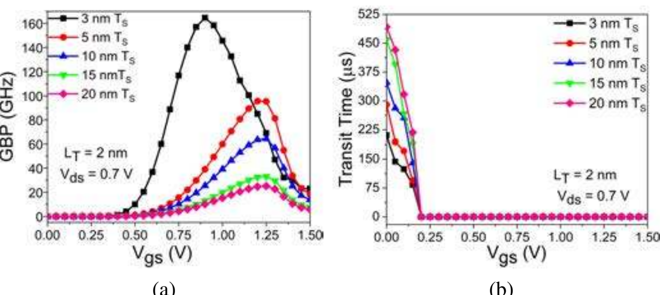

(a) (b)

Fig. 15. Analysis of (a) GBP and (b) Transit time for T_S = 3 nm to 20 nm at L_T = 2 nm

The transit time is used to verify the device speed and it is inversely related to f_t. From Fig.15b, transit time reduces as well as T_S is minimized. When T_S is set to 3 nm, we obtain lowest transit time due to high f_t, as mention in Fig.14b. For T_S variation, TFP and TGF curves are shown in Fig.16a and 16b respectively. Both the parameter directly proportional to g_m. Hence, both the parameters obtain a high value at 3 nm T_S.

3) Impact of Source Thickness (T_S) at 4 nm L_T: In this section, the consequence of T_S variation on different device parameters is analyzed when L_T is set to 4 nm. In the previous section, we had analyzed the impact of source thickness variation w.r.t 2 nm L_T, but in this case, L_T is set to 4 nm due to this the tunneling width at SCIn is increased. This effect reflects in terms of increased or decreased device parameters values. From Fig.17, for I_{ON}, V_{ON}, and steepness of $I_{ds} - V_{gs}$ curve at 3 nm T_S, the considerable deviation can be observed. Along with, for 5 nm to 20 nm of T_S, I_{ON} is decreased

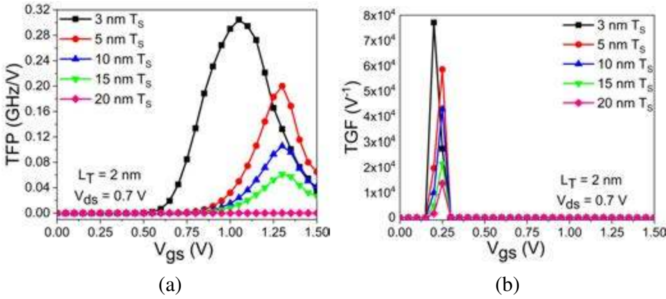

(a) (b)

Fig. 16. (a) TFP and (b) TGF curve for T_S = 3 nm to 20 nm at L_T = 2 nm for proposed device.

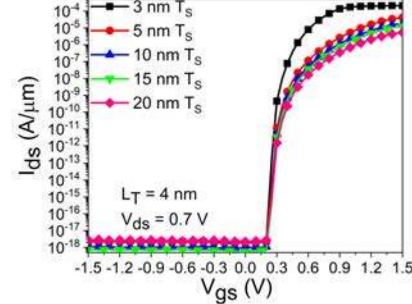

Fig. 17. Comparison of I_{ds} w.r.t V_{gs} for different T_S values at L_T = 4 nm

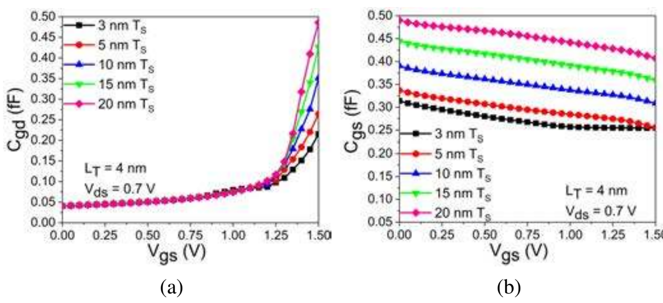

(a) (b)

Fig. 18. Analysis of (a) C_{gd} and (b) C_{gs} for T_S = 3 nm to 20 nm at L_T = 4 nm for proposed device.

compared to 2 nm L_T, as described earlier in Fig.12. As the tunneling width increase, the dominating capacitances like C_{gd} and C_{gs} also deliberate. When T_S and L_T are set to 3 nm and 4 nm respectively, the lowest C_{gd} obtain and it will increase for high T_S value (Fig.18a). Similarly, the C_{gs} is decreased as the T_S reduced w.r.t V_{gs}, as depicted in Fig.18b.

Another critical device performance parameter is g_m, which represents the amplification quality of the device. The g_m is initially increased and strikes the maximum value and then starts decreasing because, at higher V_{gs}, C_{gd} is dominating parameter, as shown in Fig.19a. The increased tunneling width does not produce any significant effect on g_m value. For frequency analysis, f_t and GBP are crucial parameters. From Fig.19b, f_t values increase at high V_{gs} for various T_S, and it attains peak its value at lower V_{gs} because g_m is dominating parameter. But, after attaining the peak value, it starts decreasing due to the high value of $(C_{gd} + C_{gs})$.

Fig.20a shows GBP versus V_{gs} graph for different T_S. The

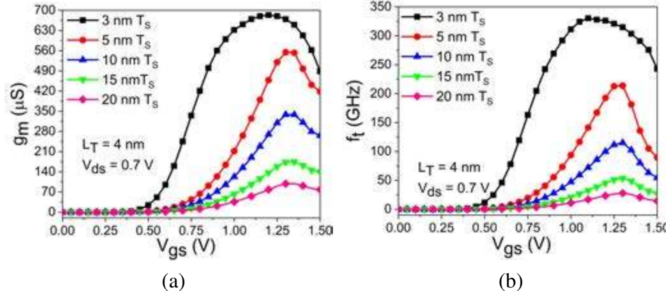

(a) (b)

Fig. 19. Data plot of (a) g_m and (b) f_t for different values of T_S at fixed L_T = 4 nm

simulation results indicate increased GBP with increased V_{gs} and the peak point is shifted towards lower gate voltage as T_S decreases. At L_T = 4 nm, the device transit delay is increased for low gate voltage compare to L_T = 2 nm for T_S variation, as display in Fig.20b.

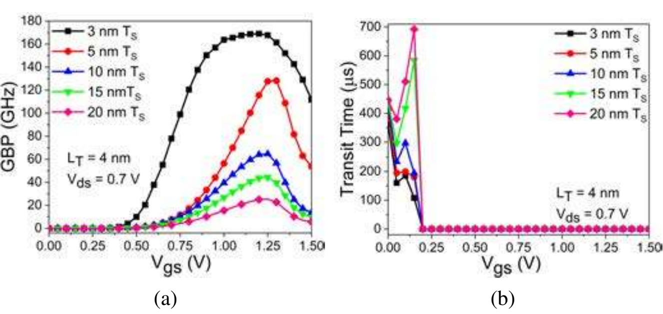

(a) (b)

Fig. 20. Analysis data plot of (a) GBP and (b) Transit time for T_S = 3 nm to 20 nm at fixed L_T = 4 nm

TFP determines the device performance at the operating frequency. It shows the relationship between power and bandwidth for high speed device applications. Ultra thin source (3nm) produces high TFP (Fig.21a) when L_T is set to 4 nm. Further, to examine the device's ability to convert power into speed, we can evaluate the TGF parameter. The higher value of TGF rewired for high speed of the device. Hence the appropriate TGF value is selected at 3nm source thickness, as shown in Fig.21b.

To clarify and to select the optimized value of L_T (2 nm or 4 nm) with optimized source thickness, a comparative analysis is performed w.r.t SS_{avg} and V_{ON} at different T_S values. The lowest value of V_{ON} is achieved at T_S = 3 nm and L_T = 4 nm, but as well as the T_S increases the V_{ON} is higher for 4 nm L_T as compared to 2 nm of L_T, mention in Fig.22a. Same way, the SS_{avg} of the device examines at different T_S when L_T set to 2 nm and 4 nm. from Fig.22b, we can see that SS_{avg} is minimum for T_S = 3 nm and L_T = 4 nm. But, the SS_{avg} for higher source thickness is high for L_T = 4 nm.

C. Optimization of Device Lateral Length

For future aspect, it is influential to analyze the scaling perceptiveness of SG-F-TFET. The channel length (L_C and L_{C1}) is already selected very carefully to get superior performance of proposed device, but the drain and source lateral length is

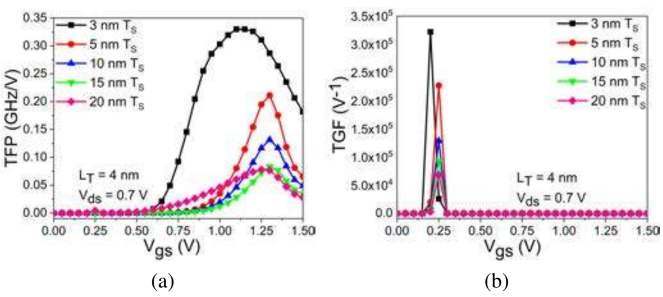

Fig. 21. (a) TFP and (b) TGF analysis curve for different values of T_S when L_T set to 4 nm for proposed device.

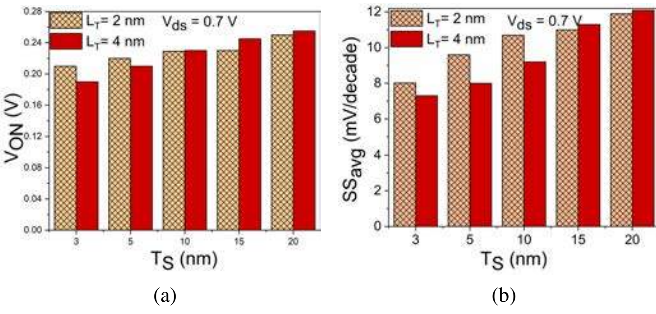

Fig. 22. A grouped bar diagram of (a) V_{ON} and (b) SS_{avg} at L_T = 2 nm and L_T = 4 nm w.r.t source thickness variation from 3 nm to 20 nm.

consider w.r.t. comparative analysis. So, the down scaling is performed on L_S and L_D to optimize the total device length without affecting its performance.

1) Down Scaling of Source Lateral Length (L_S): In this sub-section, we will figure out the optimal value of the L_S such that the characteristics of the device are not severely affected. Fig.23a and 23b shows the electric field strength at SCIn and $I_{ds} - V_{gs}$ curve of the SG-F-TFET w.r.t. changes in the L_S from 60 nm to 35 nm. Fig.22a shows that as the L_S decreased up to 40 nm, there is no effect on the electric field strength. However, as L_S is decreased below 40 nm, the electric field start decreasing. Because of this decrement in electric field the I_{ON} current of the device also start decreasing with increased V_{ON}, as shown in Fig.23b. The impact of down-scaling of source lateral length also analyzed on the capacitances like C_{gd} and C_{gs}. From Fig.24a and 24b, we can see that for L_S lower than 40 nm the capacitances are increased because of the very high accumulation of carrier near the SCIn with application of the high gate voltage. So, considering the above observation related to source lateral length optimization, we conclude that L_S = 40 nm is needed for the optimal performance of SG-F-TFET (proposed device).

2) Down Scaling of Drain Lateral Length (L_D): In this sub-section, we will find out minimum value of L_D such that the device characteristics are uninfluenced significantly. Initially, the drain lateral length set to 58 nm in proposed device. Fig.25a shows the electric field variation at DCIn of proposed device, it is remain unchanged until L_D value goes below 38 nm. For 38 nm L_D, change in electric field strength not significant. On the other hand, the I_{ON} is not significantly change from 58 nm to 38 nm of L_D. But,lower than 38 nm,

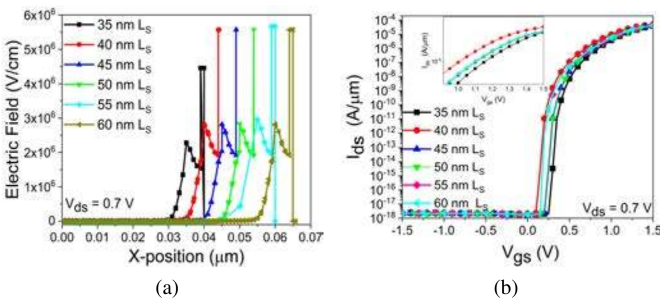

Fig. 23. Source length optimization of SG-F-TFET (a) Electric field strength analysis curve (at SCIn) and (b) I_{ds} w.r.t V_{gs} at fixed L_T = 4 nm, T_S = 3 nm, L_D = 68 nm, and SiO_2 selected as gate oxide. Inset: an enlarged $I_{ds} - V_{gs}$ graph to improve the visibility for better analysis.

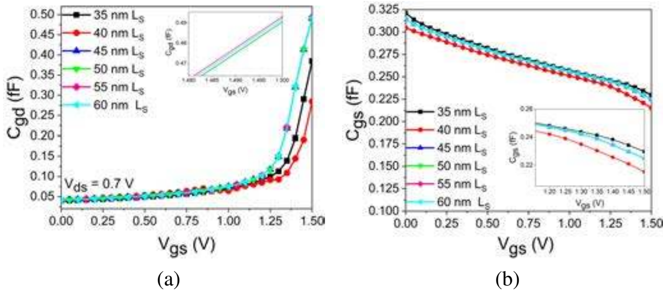

Fig. 24. (a) C_{gd} and (b) C_{gs} curves at various L_S to optimize the proposed device lateral length. Inset: an magnified $C_{gd} - V_{gs}$ and $C_{gs} - V_{gs}$ graph to improve the visibility for better analysis.

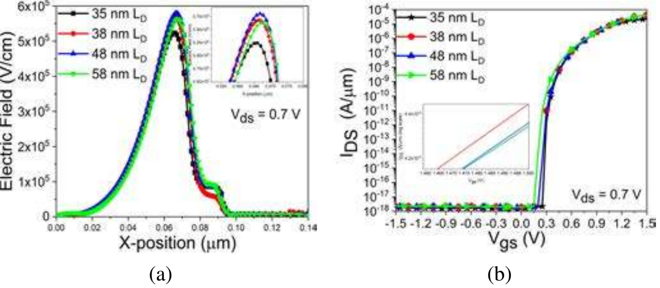

Fig. 25. Drain length optimization of SG-F-TFET (a) Electric field strength analysis curve (at DCIn)w.r.t x-axis position and (b) I_{ds} w.r.t V_{gs} at fixed L_T = 4 nm, T_S = 3 nm,L_S = 40 nm, and SiO_2 selected as gate oxide. Inset:an enlarged $I_{ds} - V_{gs}$ graph to improve the visibility for better analysis.

i.e., for L_D = 35 nm, the V_{ON} and I_{ON} decreased which are considerable change to degrade the device performance (Fig.25b).

To examine the effect of down-scaling of L_D on device performance with respect to capacitances of device, we also analyze the C_{gd} and C_{gs} for different range of L_D. The C_{gd} remain unchanged up to L_D = 38 nm, after this its value suddenly become very high (Fig.26a) because the carrier collected from the channel become very high near the DCIn region which are responsible for the gate to drain capacitances. But, the opposite effect can be seen for C_{gs}, it is remain unchanged until L_D scaled down to 38 nm and after this its value sudden fallen down in the range of 0.19 fF. The down scaling of L_D shows opposite impact on the C_{gd} and C_{gs}. As we know, the impact of C_{gd} is more dominant than C_{gs}

TABLE II
OPTIMIZED ANALOG/RF PARAMETERS OF PROPOSED DEVICE (SG-F-TFET)

Parameters	I_{ds}(A/μm)	g_m(μS)	C_{gd}(fF)	C_{gs}(fF)	f_t(GHz)	GBP(GHz)	TGF(MV^{-1})	TFP(GHz/V)	Transit time(μs)
SG-F-TFET	4.36×10^{-4}	825	0.31	0.24	370	176	0.684	0.36	215

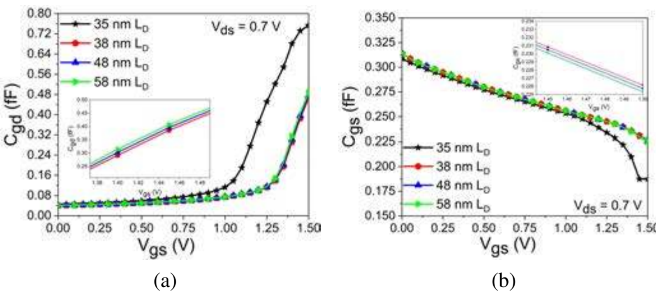

(a) (b)

Fig. 26. Analysis of (a) C_{gd} and (b) C_{gs} at various L_D to optimize the proposed device lateral length. Inset: an magnified $C_{gd} - V_{gs}$ and $C_{gs} - V_{gs}$ graph to improve the visibility for better analysis.

on device performance. Hence, the optimum value of L_D is determined as 38 nm.

V. OPTIMIZED SG-F-TFET

In section 4 (B), we have optimize the parameters (L_T, T_S), which can affect the electric field crowding effect (Electric field strength at edges of source region). Along with, in section 4 (C), device lateral length optimization have been performed and L_S and L_D are optimized. SG-F-TFET can achieve the higher drain current (A/μm) and improved analog/RF parameters as source thickness (T_S) and lateral tunneling length (L_T) decreases, as mention in figures which are listed in section 4. The optimized SG-F-TFET consists, L_T = 4 nm, T_S = 3 nm, L_D = 38 nm, L_S = 40 nm and T_{OX} set to 1 nm, SiO_2 as gate oxide material. The WF_G set ot 4.5 eV and N_S, N_C and N_D is 10^{20} cm^{-3}, 10^{15} cm^{-3} and 10^{18} cm^{-3} respectively. Considering the above optimum parameters related to dimensions, final L_{tt} of device is 103 nm with T_{tt} = 42 nm. The analog/RF parameters of optimized SG-F-TFET are listed in Table 2.

VI. CONCLUSION

A new SG-F-TFET is designed and its fundamental physics of devices and working principle are investigated in detail using the 2D TCAD simulator. The proposed modification in SG-F-TFET improves ON-state current and reduced V_{ON} with increased SS_{avg} (below 9 mV/decade), ambipolar current suppress drastically ($10^{11} order$) correspond to the DG-TFET. The results confirm that SG-F-TFET can achieve a relatively lower V_{ON} (approximately 0.3 V) with L_T = 4 nm and T_S = 3 nm. Along with these advantages, proposed device also consist low C_{gd} and C_{gs} which are causative for improved device controllability. We have also demonstrated that SG-F-TFET device is exempt to reduction in L_S and L_D up to 40 nm and 38 nm respectively. For analog/RF parameters such as C_{gs},C_{gd}, g_m, f_t, GBP, TFP, TGF and transit time are analyzed to determination the feasibility of the SG-F-TFET for high frequency application with low power operation. It was found that when the L_T, T_S, L_S and L_D set to 4 nm, 3 nm, 40 nm and 38 nm respectively, SG-F-TFET shows the better performance for high frequency parameters. At the last, SG-F-TFET is expected to be fabricated by self-aligned processes. So, optimized SG-F-TFET can be utilized as promising alternative for low power high frequency applications.

ACKNOWLEDGMENT

The authors would like to thank Dr. Dip Prakash Samajdar from Department of Electronics and Communication Engineering, PDPM Indian Institute of Information Technology, Design and Manufacturing, Jabalpur, Madhya Pradesh, India for providing valuable suggestions and support to carry out this research work.

REFERENCES

[1] U. E. Avci, D. H. Morris, and I. A. Young, "Tunnel field-effect transistors prospects and challenges," *IEEE Journal of the Electron Devices Society*, vol. 3, no. 3, pp. 88–95, 2015.

[2] A. M. Ionescu and H. Riel, "Tunnel field-effect transistors as energy-efficient electronic switches," *nature*, vol. 479, no. 7373, pp. 329–337, 2011.

[3] K. Boucart and A. M. Ionescu, "Double-gate tunnel fet with high-k gate dielectric," *IEEE transactions on electron devices*, vol. 54, no. 7, pp. 1725–1733, 2007.

[4] E.-H. Toh, G. H. Wang, L. Chan, G. Samudra, and Y.-C. Yeo, "Device physics and guiding principles for the design of double-gate tunneling field effect transistor with silicon-germanium source heterojunction," *Applied Physics Letters*, vol. 91, no. 24, p. 243505, 2007.

[5] B. R. Raad, D. Sharma, P. Kondekar, K. Nigam, and D. S. Yadav, "Drain work function engineered doping-less charge plasma tfet for ambipolar suppression and rf performance improvement: a proposal, design, and investigation," *IEEE Transactions on Electron Devices*, vol. 63, no. 10, pp. 3950–3957, 2016.

[6] A. Mallik, A. Chattopadhyay, S. Guin, and A. Karmakar, "Impact of a spacer–drain overlap on the characteristics of a silicon tunnel field-effect transistor based on vertical tunneling," *IEEE transactions on electron devices*, vol. 3, no. 60, pp. 935–943, 2013.

[7] D. S. Yadav, D. Sharma, B. R. Raad, and V. Bajaj, "Dual workfunction hetero gate dielectric tunnel field-effect transistor performance analysis," in *2016 International Conference on Advanced Communication Control and Computing Technologies (ICACCCT)*. IEEE, 2016, pp. 26–29.

[8] A. Villalon, G. Le Carval, S. Martinie, C. Le Royer, M.-A. Jaud, and S. Cristoloveanu, "Further insights in tfet operation," *IEEE Transactions on Electron Devices*, vol. 61, no. 8, pp. 2893–2898, 2014.

[9] S. Garg and S. Saurabh, "Exploiting within-channel tunneling in a nanoscale tunnel field-effect transistor," *IEEE Open Journal of Nanotechnology*, vol. 1, pp. 100–108, 2020.

[10] D. B. Abdi and M. J. Kumar, "In-built n+ pocket pnpn tunnel field-effect transistor," *IEEE Electron Device Letters*, vol. 35, no. 12, pp. 1170–1172, 2014.

[11] S. Tirkey, B. R. Raad, A. Gedam, and D. Sharma, "Junction-less charge plasma tfet with dual drain work functionality for suppressing ambipolar nature and improving radio-frequency performance," *Micro & Nano Letters*, vol. 13, no. 1, pp. 18–23, 2018.

[12] W. Cao, C. Yao, G. Jiao, D. Huang, H. Yu, and M.-F. Li, "Improvement in reliability of tunneling field-effect transistor with pnin structure," *IEEE transactions on electron devices*, vol. 58, no. 7, pp. 2122–2126, 2011.

[13] R. Narang, M. Saxena, R. Gupta, and M. Gupta, "Assessment of ambipolar behavior of a tunnel fet and influence of structural modifications," *JSTS: Journal of Semiconductor Technology and Science*, vol. 12, no. 4, pp. 482–491, 2012.

[14] S. Yun, J. Oh, S. Kang, Y. Kim, J. H. Kim, G. Kim, and S. Kim, "F-shaped tunnel field-effect transistor (tfet) for the low-power application," *Micromachines*, vol. 10, no. 11, p. 760, 2019.
[15] J. Fossum, J.-W. Yang, and V. Trivedi, "Suppression of corner effects in triple-gate mosfets," *IEEE Electron Device Letters*, vol. 24, no. 12, pp. 745–747, 2003.
[16] A. U. Manual, "Silvaco international inc," *Santa Clara, Ca, USA*, 2016.
[17] S. Tirkey, D. Sharma, B. R. Raad, and D. S. Yadav, "A novel approach to improve the performance of charge plasma tunnel field-effect transistor," *IEEE Transactions On Electron Devices*, vol. 65, no. 1, pp. 282–289, 2017.
[18] R. M. Imenabadi, M. Saremi, and W. G. Vandenberghe, "A novel pnpn-like z-shaped tunnel field-effect transistor with improved ambipolar behavior and rf performance," *IEEE transactions on electron devices*, vol. 64, no. 11, pp. 4752–4758, 2017.
[19] S. Tirkey, D. S. Yadav, and D. Sharma, "Controlling ambipolar behavior and improving radio frequency performance of hetero junction double gate tfet by dual work-function, hetero gate dielectric, gate underlap: Assessment and optimization," in *2017 International Conference on Information, Communication, Instrumentation and Control (ICICIC)*. IEEE, 2017, pp. 1–7.
[20] R. G. Debnath, K. Baruah, and S. Baishya, "Dc and analog/rf performance analysis of gate extended u-shaped channel tunnel field effect transistor," *Microsystem Technologies*, vol. 26, no. 9, pp. 2793–2799, 2020.
[21] C. Pandey, D. Dash, and S. Chaudhury, "Improvement in analog/rf performances of soi tfet using dielectric pocket," *International Journal of Electronics*, vol. 107, no. 11, pp. 1844–1860, 2020.
[22] D. S. Yadav, D. Sharma, B. R. Raad, and V. Bajaj, "Impactful study of dual work function, underlap and hetero gate dielectric on tfet with different drain doping profile for high frequency performance estimation and optimization," *Superlattices and Microstructures*, vol. 96, pp. 36–46, 2016.
[23] D. Shekhar and A. Raman, "Design and analysis of dual-gate misalignment on the performance of dopingless tunnel field effect transistor," *Applied Physics A*, vol. 126, pp. 1–9, 2020.
[24] N. Guenifi, S. Rahi, and M. Larbi, "Suppression of ambipolar current and analysis of rf performance in double gate tunneling field effect transistors for low-power applications," *Int J Nanoparticles Nanotech*, vol. 6, p. 033, 2020.
[25] D. S. Yadav, B. R. Raad, and D. Sharma, "A novel gate and drain engineered charge plasma tunnel field-effect transistor for low sub-threshold swing and ambipolar nature," *Superlattices and Microstructures*, vol. 100, pp. 266–273, 2016.
[26] N. Abraham and R. K. James, "An improved tunnel field-effect transistor with an l-shaped gate and channel," *Journal of Computational Electronics*, vol. 19, no. 1, pp. 304–309, 2020.
[27] S. Saurabh and M. J. Kumar, "Novel attributes of a dual material gate nanoscale tunnel field-effect transistor," *IEEE transactions on Electron Devices*, vol. 58, no. 2, pp. 404–410, 2010.
[28] D. Shekhar and A. Raman, "Tweaking the performance of dopingless nano-tfet with misaligned sandwiched dual-gate structure," *Silicon*, pp. 1–11, 2021.
[29] T. Joshi, B. Singh, and Y. Singh, "Controlling the ambipolar current in ultrathin soi tunnel fets using the back-bias effect," *Journal of Computational Electronics*, vol. 19, no. 2, pp. 658–667, 2020.
[30] S. W. Kim, J. H. Kim, T.-J. K. Liu, W. Y. Choi, and B.-G. Park, "Demonstration of l-shaped tunnel field-effect transistors," *IEEE transactions on electron devices*, vol. 63, no. 4, pp. 1774–1778, 2015.
[31] K.-H. Kao, A. S. Verhulst, W. G. Vandenberghe, B. Soree, W. Magnus, D. Leonelli, G. Groeseneken, and K. De Meyer, "Optimization of gate-on-source-only tunnel fets with counter-doped pockets," *IEEE Transactions on Electron Devices*, vol. 59, no. 8, pp. 2070–2077, 2012.
[32] C. Anghel, P. Chilagani, A. Amara, and A. Vladimirescu, "Tunnel field effect transistor with increased on current, low-k spacer and high-k dielectric," *applied physics letters*, vol. 96, no. 12, p. 122104, 2010.
[33] S. Saurabh and M. J. Kumar, *Fundamentals of tunnel field-effect transistors*. CRC press, 2016.
[34] Z. Yang, "Tunnel field-effect transistor with an l-shaped gate," *IEEE electron device letters*, vol. 37, no. 7, pp. 839–842, 2016.
[35] Y. Zhu and M. K. Hudait, "Low-power tunnel field effect transistors using mixed as and sb based heterostructures," *Nanotechnology Reviews*, vol. 2, no. 6, pp. 637–678, 2013.